Chapter 5

Prestack migration using the LITWEQ method

Although common-midpoint stacking (Mayne, 1962) has the advantage of improving signal-to-noise ratios and reducing data sizes before migration, it also has the disadvantage of averaging reflectivities over certain segments of reflectors when reflectors are dipping, or when the earth is laterally inhomogeneous. This averaging of reflectivities distorts pictures of underground structures, in particular obscuring details of reflectivity changes so that analysis of seismic stratigraphy becomes difficult. Other disadvantages of CMP stacking include data aliasing (of dipping and overturned reflections) in CMP gathers, and high computer I/O expense for sorting CMP gathers. To overcome these problems, prestack migration (i.e., imaging before stacking) (Claerbout, 1976; Jacobs, 1982) and partial prestack migration (i.e., dip-moveout) (Judson et al., 1978; Hale, 1983) have been introduced in the seismic industry over the years.

As an application of the LITWEQ method, LITWEQ prestack profile migration will be discussed in this chapter. Prospects for further applications of the LITWEQ method also will be summarized.

§ 5.1 PROFILE MIGRATION USING THE LITWEQ METHOD

Forward modeling

Shot profile migration consists of matching a forward modeling of a downgoing wavefield (generated by a given velocity and source model) with a backward extrapolation of upcoming reflections (recorded at the earth's surface). Consequently, LITWEQ forward modeling is required only in the region enclosed by three lines: $t_1 = (t + \tau)/\sqrt{2} = t_{\max}/\sqrt{2}$, $t_1 = t_2$ and $t_1 = -t_2$, where $t_{\max}$ is the maximum record time and τ is the pseudo-depth. The computation can be further reduced to the region enclosed by $t_1 = t_{\max}/\sqrt{2}$, $t_2 = \tau_{smax}/\sqrt{2}$, $t_1 = t_2$ and $t_1 = -t_2$ (see Figure 5.1), if the maximum pseudo-depth of the source is τ_{smax}. It is obvious that the computation, when the source is at the surface (i.e., $\tau_{smax} = 0$), is reduced to one-fourth of

the computation for the LITWEQ two-way modeling described in section 4.3.

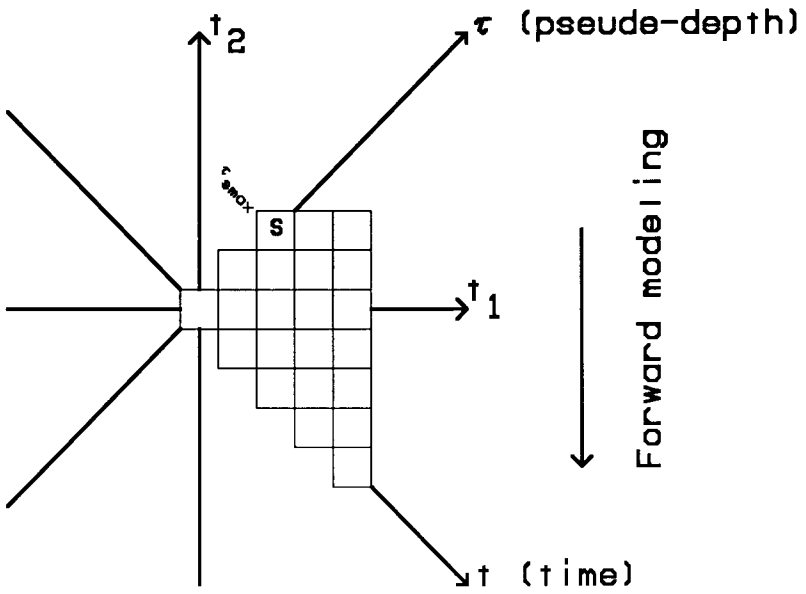

FIG. 5.1. Computation grids for finite-difference LITWEQ forward modeling of down-going waves in the (t_1, t_2) plane. The maximum depth of the source location is at $\tau = \tau_{smax}$. The source is denoted by S. For a surface source, $\tau_{smax} = 0$, computation can be reduced to those grids in the figure with $t_2 \leq 0$.

Backward extrapolation

With the wavefield $P(x, t_1{=}t/\sqrt{2}, t_2{=}{-}t/\sqrt{2})$ recorded at the earth's surface, the backward (in time) extrapolation of $P(x, t_1, t_2)$ in the LITWEQ coordinates is carried out in the region enclosed by $t_1 = t_{\max}/\sqrt{2}$, $t_2 = \tau_{smax}/\sqrt{2}$, $t_1 = t_2$ and $t_1 = -t_2$ (see Figure 5.2).

Because some reflections (dipping-bed reflections) in a seismic profile may come from reflectors whose locations are outside the profile, some traces should be padded at both sides of the profile before forward modeling and backward extrapolating, especially on the near-offset side. The number of traces that need to be padded depends on both the angles of the dipping reflectors and the velocity distribution. In backward extrapolation, to enhance the resolution of imaging it is better to pad seismic traces

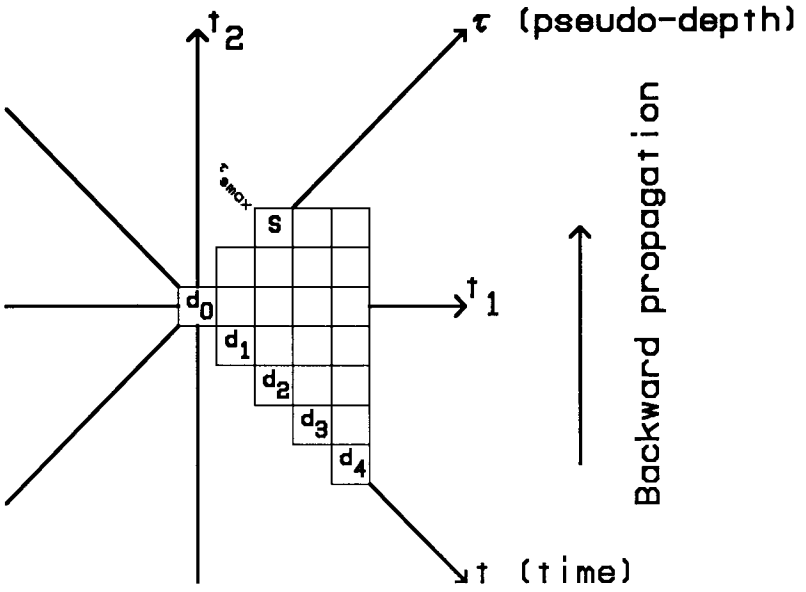

FIG. 5.2. Computation grids for finite-difference LITWEQ backward extrapolation of upcoming reflections in the (t_1, t_2) plane. The surface data are denoted by d_i's.

selected from other shot profiles, according to reciprocity of source and receiver, than to pad traces of all zeros. However, interpolation between these padded traces is probably necessary unless receiver spacing is equal to an integer multiple of shot spacing.

Imaging by zero-lag cross-correlation

After the above two processes (forward modeling and backward extrapolation) are completed, a migrated profile can be obtained by correlating the two separate wavefields.

For any moment t at any underground position (x, z), the reflected wavefield $B(x, z, t)$ (the result of backward extrapolation) must be equal to the incident wavefield $F(x, z, t)$ (the result of forward modeling) times the reflectivity $C(x, z)$; i.e.,

$$B(x, z, t) = F(x, z, t)\, C(x, z)\,. \tag{5.1}$$

Since the reflectivity is time-independent (the physical properties of the earth do not change during the survey), $C(x, z)$ can be estimated by the least-squares

principle, giving

$$C_0(x\,,\,z) \;=\; \frac{1}{NT}\sum_{it=1}^{NT}\frac{B(x\,,\,z\,,\,it)}{F(x\,,\,z\,,\,it)}\,, \tag{5.2}$$

where NT is the number of time samples per trace. This summation over the time axis, to estimate reflectivity, enhances coherent images of primary reflections, while suppressing incoherent noise. If a ray-tracing algorithm is used in computing the arrival time t, the summation over the time axis should start from t and end at $t + T_w$, where T_w is the time duration of the seismic wavelet used in the survey.

Estimation of reflectivity using equation (5.2) is usually unstable because small values of $F(x\,,\,z\,,\,t)$ cause overflow problems in computation. Three other approximate, but feasible, estimates of $C(x\,,\,z)$ from time-dependent data $B(x\,,\,z\,,\,t)$ and $F(x\,,\,z\,,\,t)$ are summarized as follows, analogously to Jacobs' Fourier-domain estimates (Jacobs, 1982):

$$C_1(x\,,\,z) \;=\; \frac{1}{NT}\sum_{it=1}^{NT} W(x\,,\,z\,,\,it)\,B(x\,,\,z\,,\,it)\,F(x\,,\,z\,,\,it)\,, \tag{5.3}$$

$$C_2(x\,,\,z) \;=\; \frac{1}{NT}\sum_{it=1}^{NT} W(x\,,\,z\,,\,it)\,B(x\,,\,z\,,\,it)\,\mathbf{sign}[F(x\,,\,z\,,\,it)]\,,\ \text{and} \tag{5.4}$$

$$C_3(x\,,\,z) \;=\; \frac{1}{NT}\sum_{it=1}^{NT} W(x\,,\,z\,,\,it)\,\frac{B(x\,,\,z\,,\,it)\,F(x\,,\,z\,,\,it)}{|\,F(x\,,\,z\,,\,it)\,|^{\,2}+\epsilon^2}\,, \tag{5.5}$$

where ϵ^2 is a positive small number, $W(x\,,\,z\,,\,t)$ is a weighting function depending on both the geometric spreading of wave propagation and the reliability of computed wavefields, and the sign function $\mathbf{sign}(x)$ equals $+1$ if $x > 0$, -1 if $x < 0$, and 0 if $x = 0$. Estimation of reflectivity using equations (5.2)-(5.5) is simply a zero-lag cross-correlation of the forward-modeled wavefield and the backward-extrapolated wavefield with a certain weighting function. Experiments have shown that estimation using equation (5.3) gives the best result with the least effort and is also the most robust one.

Estimate C_1 is equivalent to one of the conventional frequency-domain estimates of reflectivity, because integrating $B(t)F(t)$ over t is the same as integrating $B(\omega)F^*(\omega)$ over ω, where $B(\omega)$ is the Fourier transform of $B(t)$ and $F^*(\omega)$ is the conjugate of the Fourier transform of $F(t)$.

Synthetic results

Figure 5.3a shows a shot profile before migration. The profile contains reflections from two flat reflectors. The reflectors are well imaged in Figure 5.3b by LITWEQ prestack migration. For flat-bed reflections, images will be obtained only on the near-offset side of the profile, since the profile only records reflections from this half of the section. Data-truncation effects due to limited offsets are likely to be seen on both sides of the imaged reflectors (see Figure 5.3b). Data extrapolation (Claerbout, 1985) on both sides of unmigrated profiles should suppress these truncation artifacts.

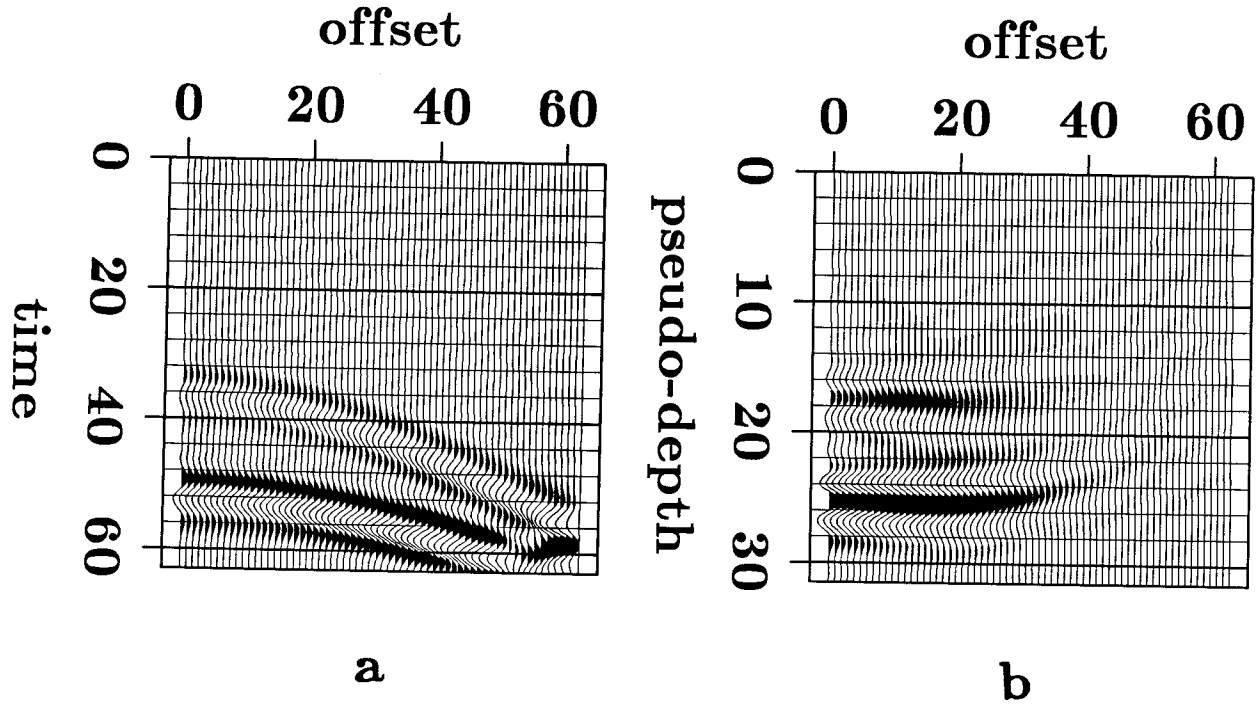

FIG. 5.3. **a.** Synthetic shot profile of reflections from a three-layer model. The thicknesses of the three layers are $\Delta\tau_1 = 17$, $\Delta\tau_2 = 7$ and $\Delta\tau_3 = \infty$. The velocities are $v_1 = 1.5$, $v_2 = 2$ and $v_3 = 3$. **b.** Migrated profile of the three-layer model.

Figure 5.4 shows a profile migration of dipping reflections. After migration, a pseudo-time-to-depth conversion is made to obtain the migrated depth section shown in Figure 5.4b. Again, the result shows that LITWEQ prestack migration works properly.

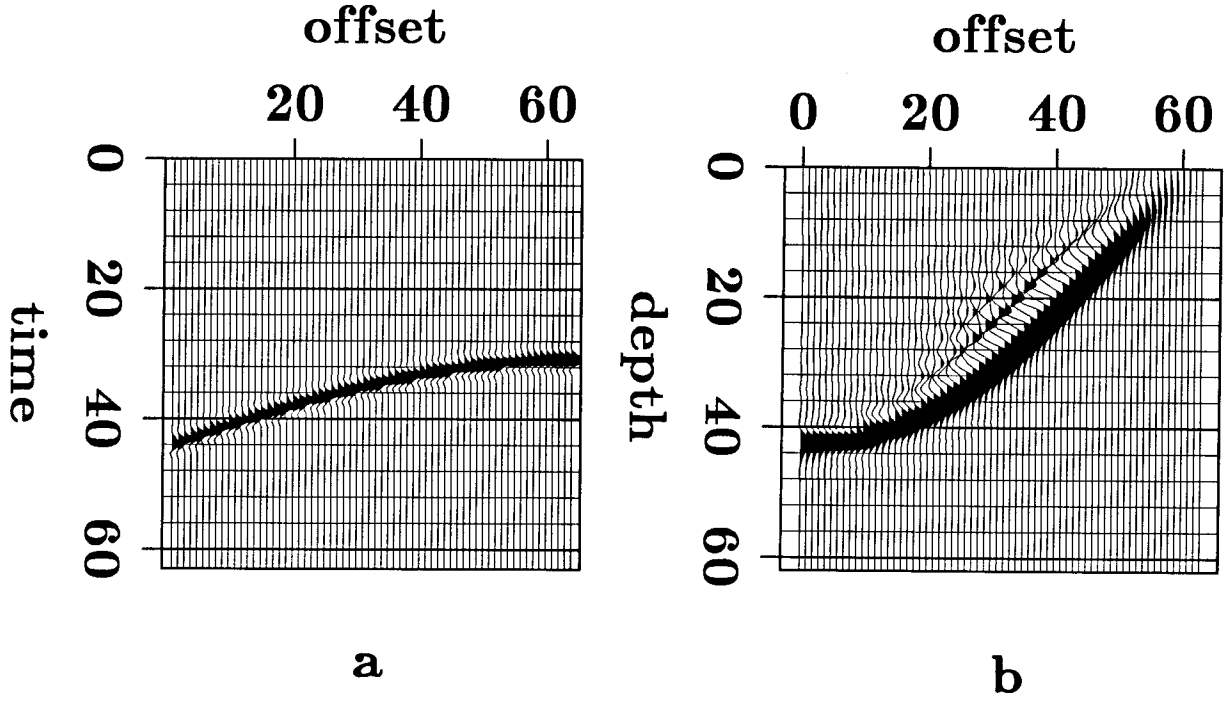

FIG. 5.4. **a.** Synthetic shot profile of reflections from a 45-degree dipping-fault-plane model. The velocity above the fault plane is $v_1 = 2$, while the velocity below is $v_2 = 3$. **b.** Migrated depth section of the fault plane. Data-truncation effects can be seen at both sides of the imaged fault plane.

Field data results

LITWEQ prestack migration was applied to 56 shot gathers from the Gulf of Mexico. The profiles contain both flat-bed and dipping-bed reflections. Figure 5.5a shows one of the shot gathers. We will pay special attention to a fault-plane reflection appearing at about 1.4 seconds on the nearest offset and at 1.3 seconds on the farthest offset (marked by **D** in Figures 5.5a and 5.5b), and to multiple reflections appearing below the primary reflection (marked by **F**) at 2.25 seconds on the nearest offset and 2.5 seconds on the farthest offset.

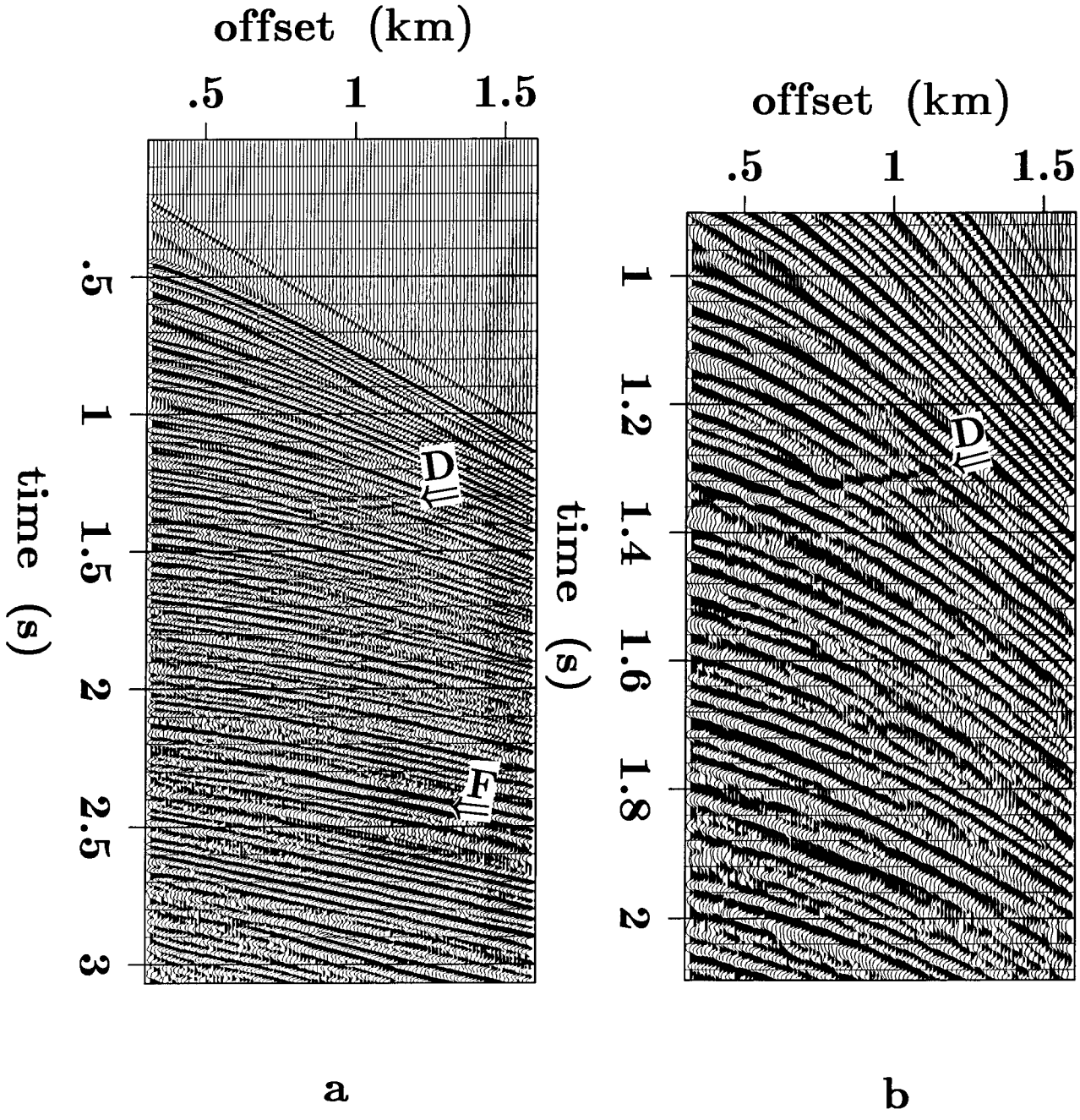

FIG. 5.5. **a.** A shot gather from the Gulf of Mexico. Reflections from a dipping fault plane can be seen at about 1.4 seconds at the nearest offset and at 1.3 seconds at the farthest offset, as marked by **D.** Some multiple reflections after a strong flat-bed reflection (marked by **F**) at about 2.25 seconds at the nearest offset and at 2.5 seconds at the farthest offset are present in the gather. **b.** Amplified display of a window of the profile in Figure 5.5a. The reflection from a fault plane (dipping to the left) can be seen clearly in the figure.

Figure 5.6 shows the migrated version of the profile of Figure 5.5a. Flat reflectors are all imaged well in the migrated section. Notice that the dipping fault plane is also nicely imaged, with high resolution, and that the multiple reflections after the imaged flat reflector at 1.1 seconds (pseudo-depth) are suppressed in the final section. Some tilted events on the right-hand side of the final section are reflections from the sides of computational grids. These boundary reflections are incoherent and hence will be reduced when we finally stack different migrated profiles, though absorbing boundary conditions should be able to suppress them.

§ 5.2 STACKING OF MIGRATED PROFILES

Each migrated profile provides a picture of a certain portion of the underground structures being studied; these pictures usually overlap with adjacent ones if shot spacing is less than half of maximum offsets (single-end spread) or half of cable length (split spread). The images in different migrated profiles will be coherent, or aligned, if the correct velocity function is used in the migration of all profiles. Stacking of these coherent images certainly enhances the resolution of the underground structures, while suppressing incoherent noise (reverberations and boundary reflections). Stacking is done with the following formula:

$$\textbf{Image}(x\,,\,z) \;=\; \sum_{is=1}^{NS} \frac{C_{is}(x\,,\,z)}{N(x)}\,, \tag{5.6}$$

where NS is the number of shots in a survey line, and $N(x)$ is the number of ray coverages in position x.

Five of the 56 migrated profiles mentioned in section 5.1 are displayed in Figure 5.7. The images of these migrated profiles are aligned exactly. Stacking over the 56 separate images offers a clearer picture of the underground structures (Figure 5.8) than that provided by any individual migrated profile. Notice again that in Figure 5.8 the dipping fault plane is well imaged, while the computational boundary reflections we saw in Figure 5.5 are suppressed.

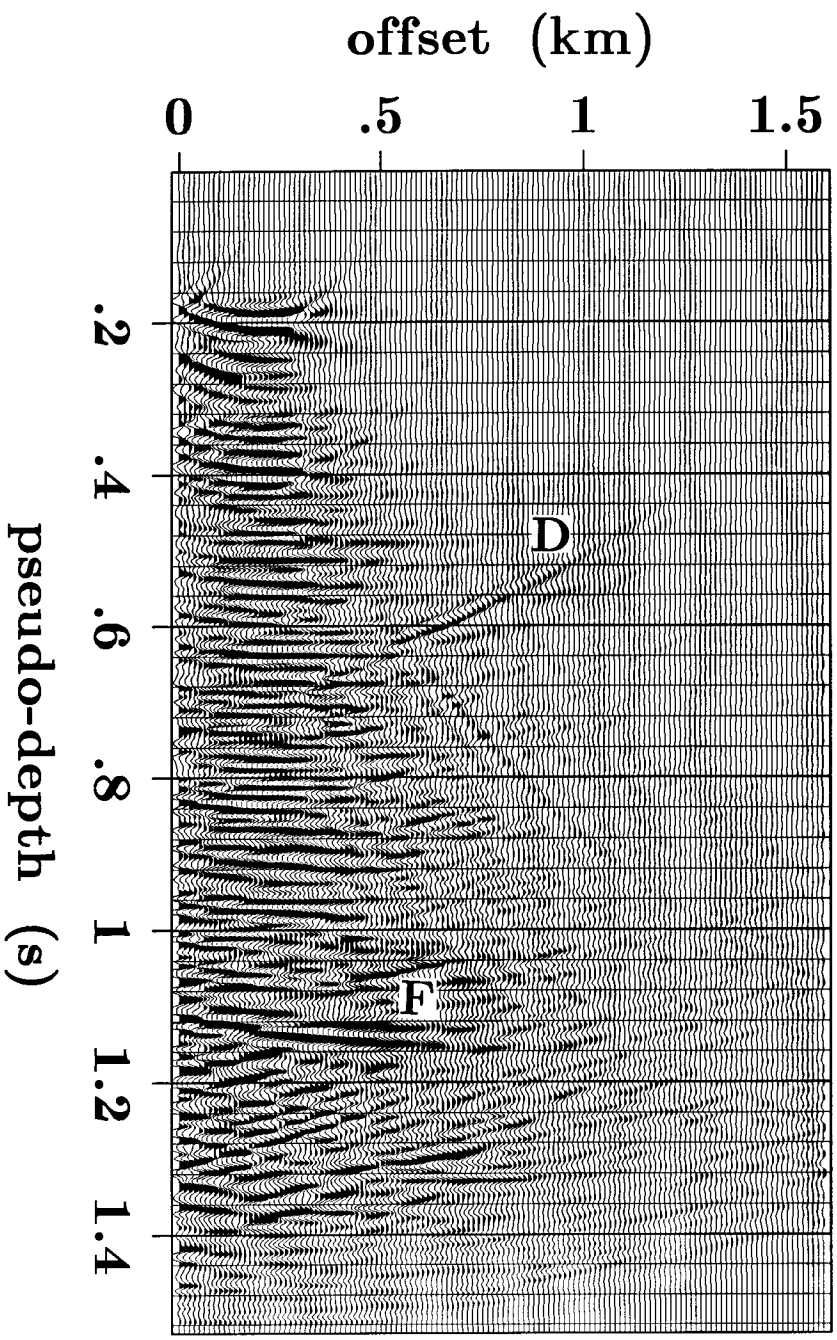

FIG. 5.6. Migrated profile of the gather in Figure 5.5. The dipping fault plane **E** is well imaged. The multiple reflections mentioned in Figure 5.5 have been suppressed in the migrated profile, while the flat-bed reflection **F** above them is migrated to about 1.1 seconds of pseudo-depth.

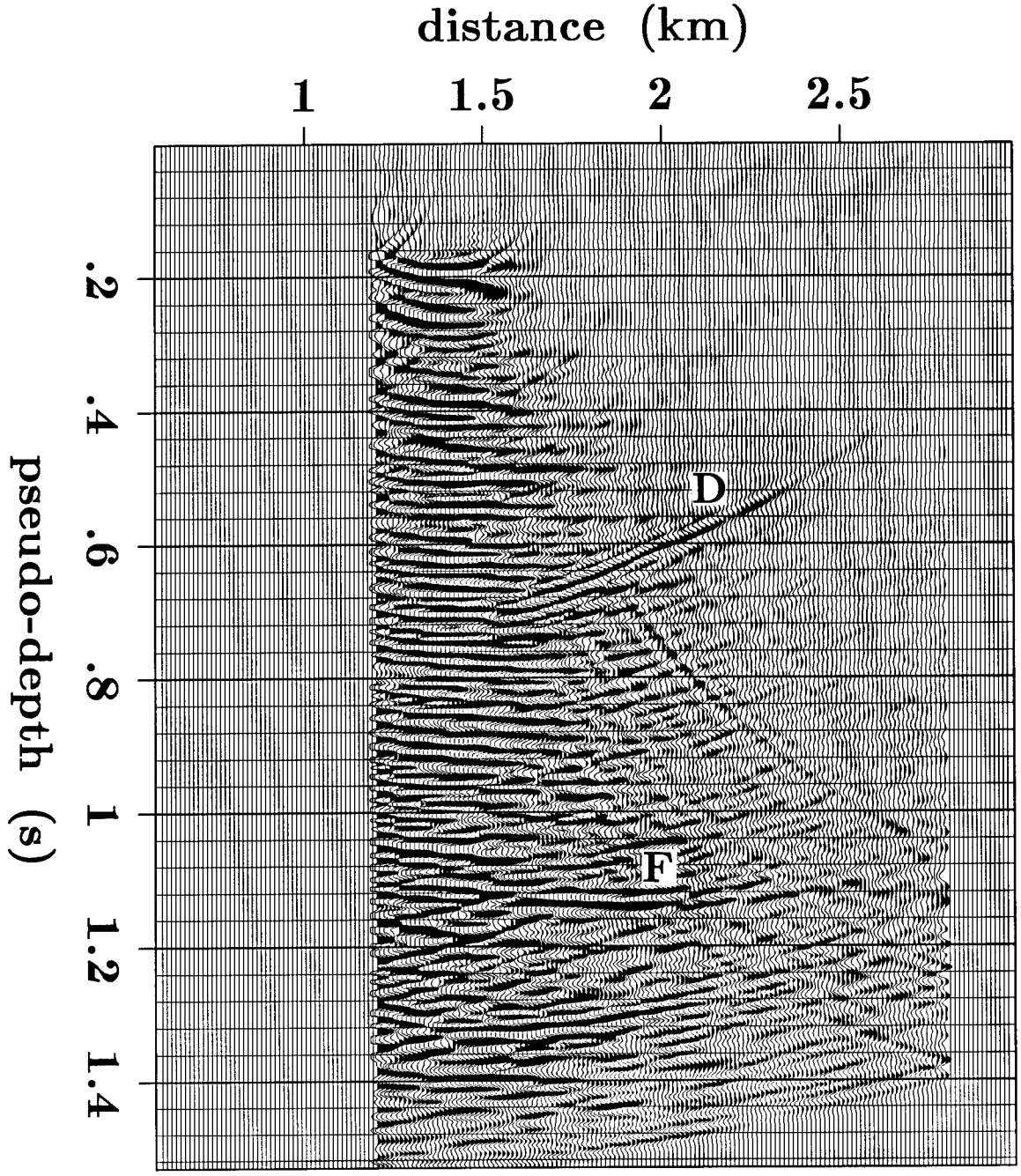

FIG. 5.7a. Migrated profile of shot gather s8.

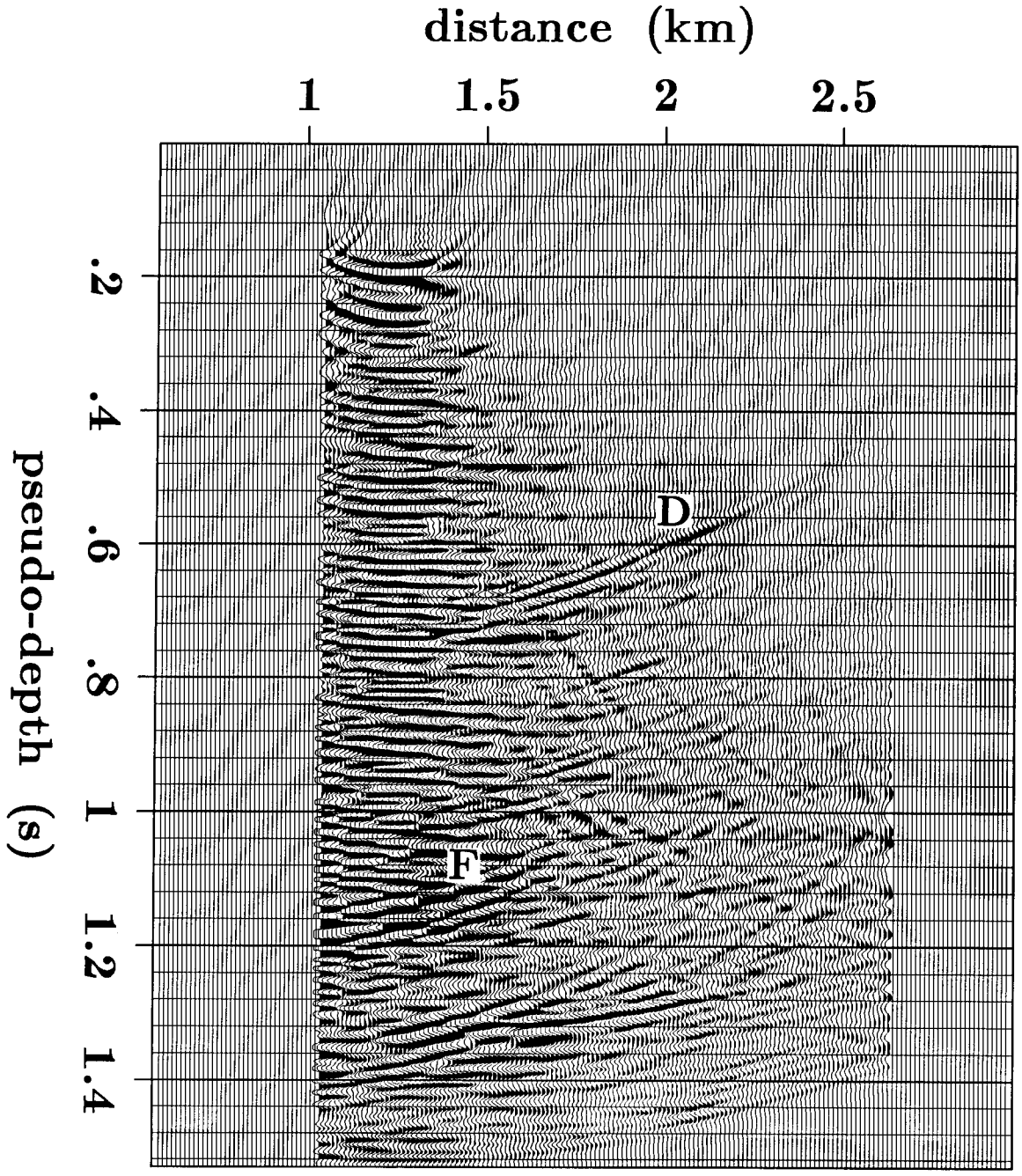

FIG. 5.7b. Migrated profile of shot gather s14.

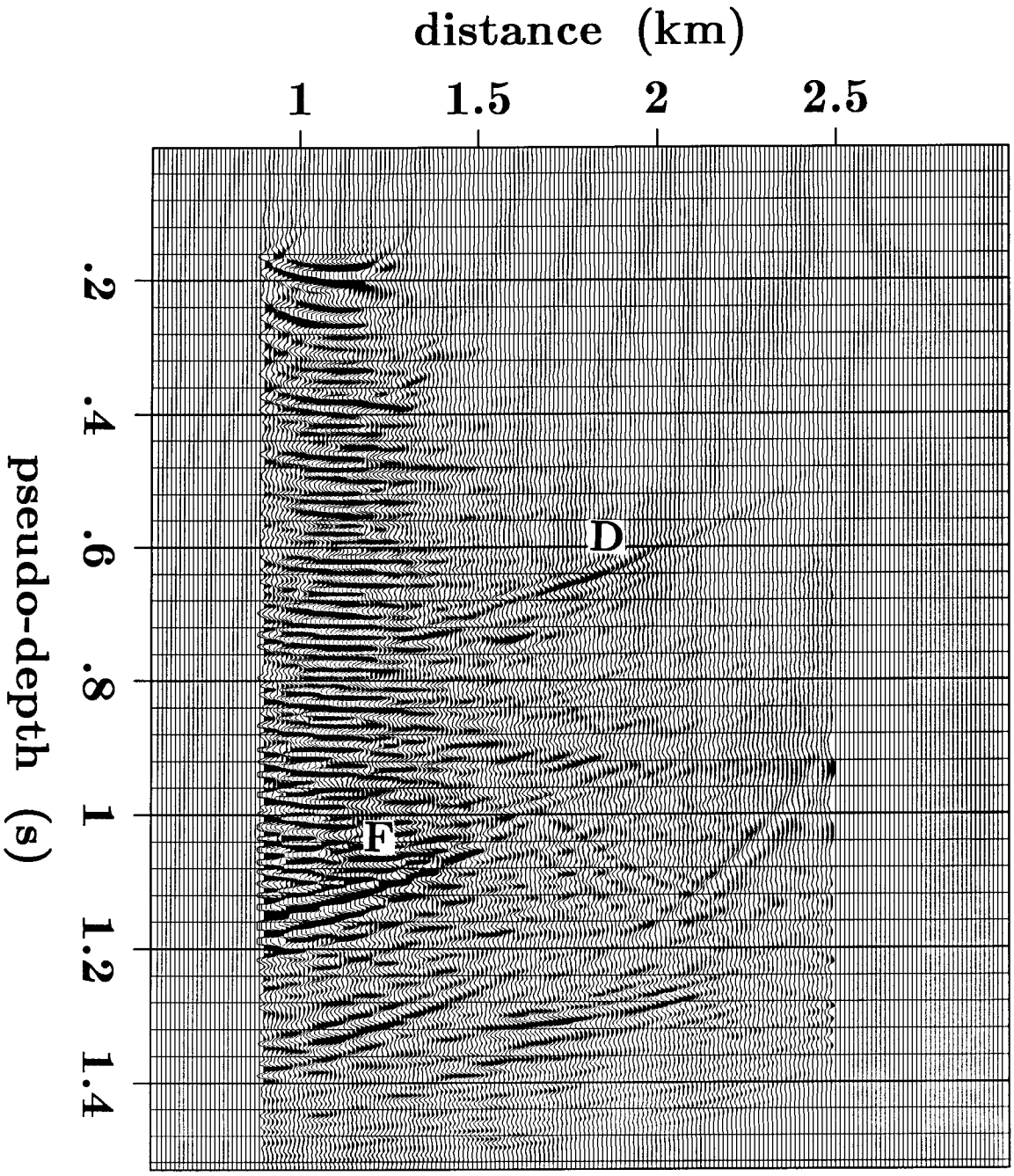

FIG. 5.7c. Migrated profile of shot gather s20.

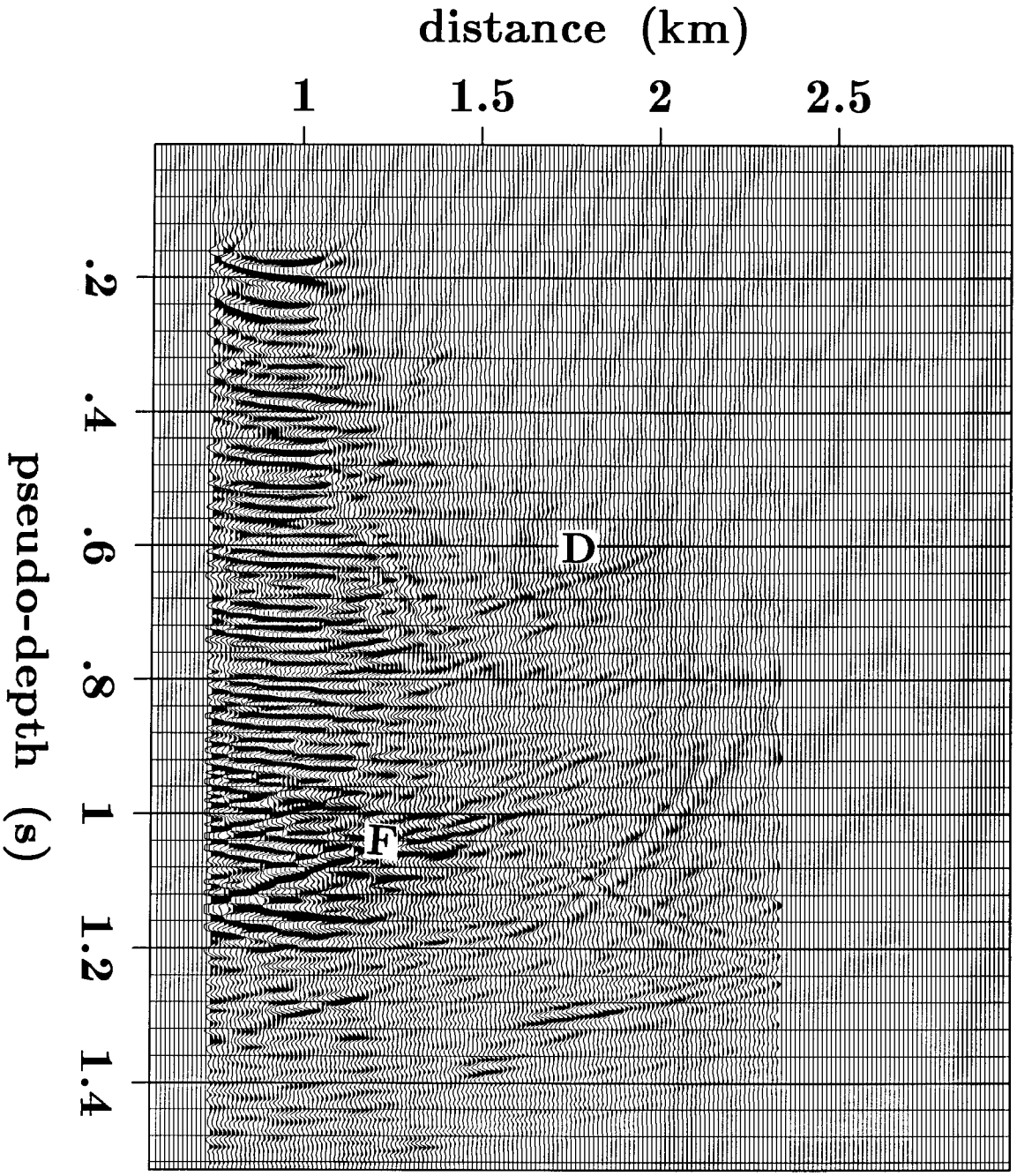

FIG. 5.7d. Migrated profile of shot gather s26.

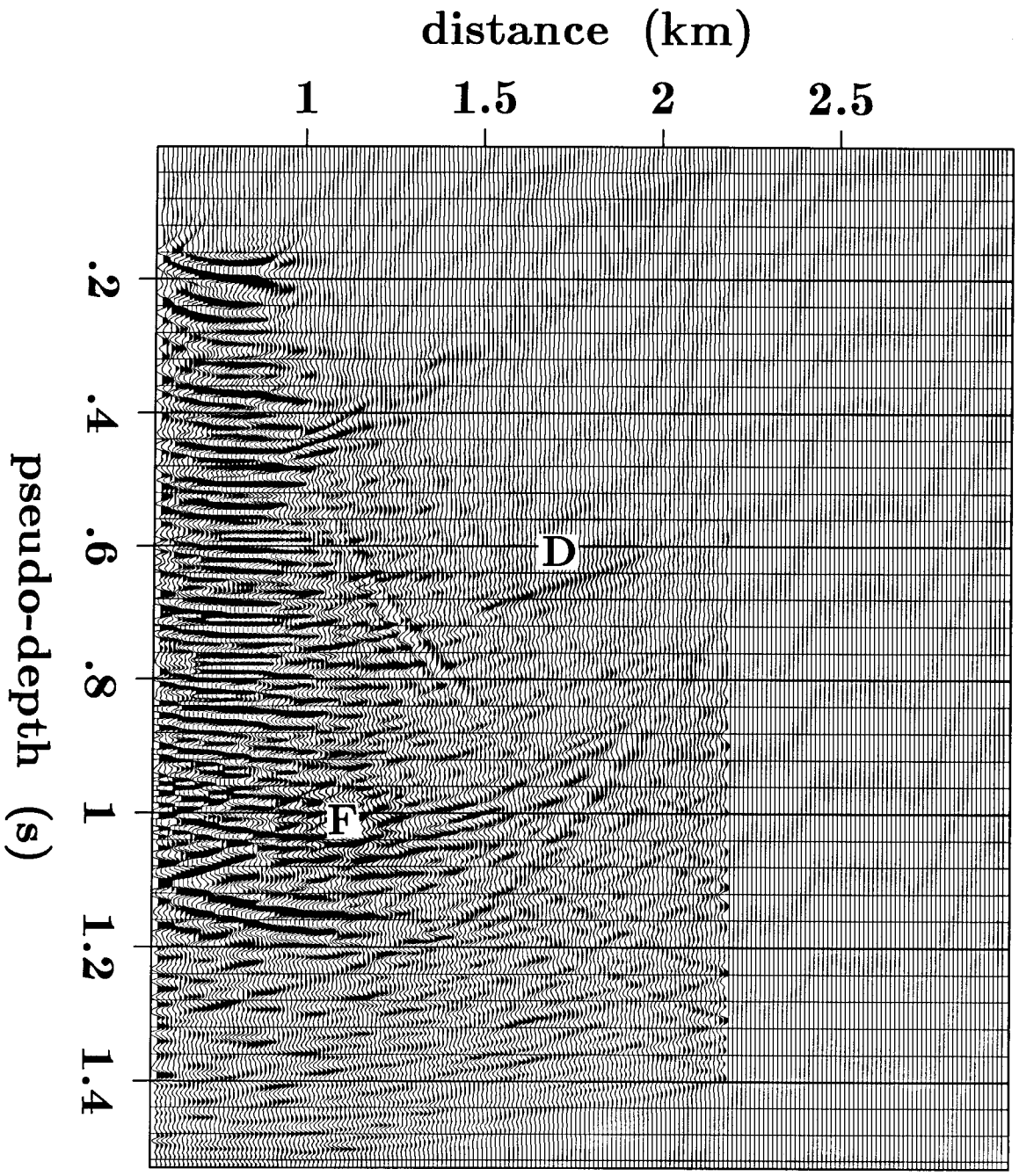

FIG. 5.7e. Migrated profile of shot gather s32.

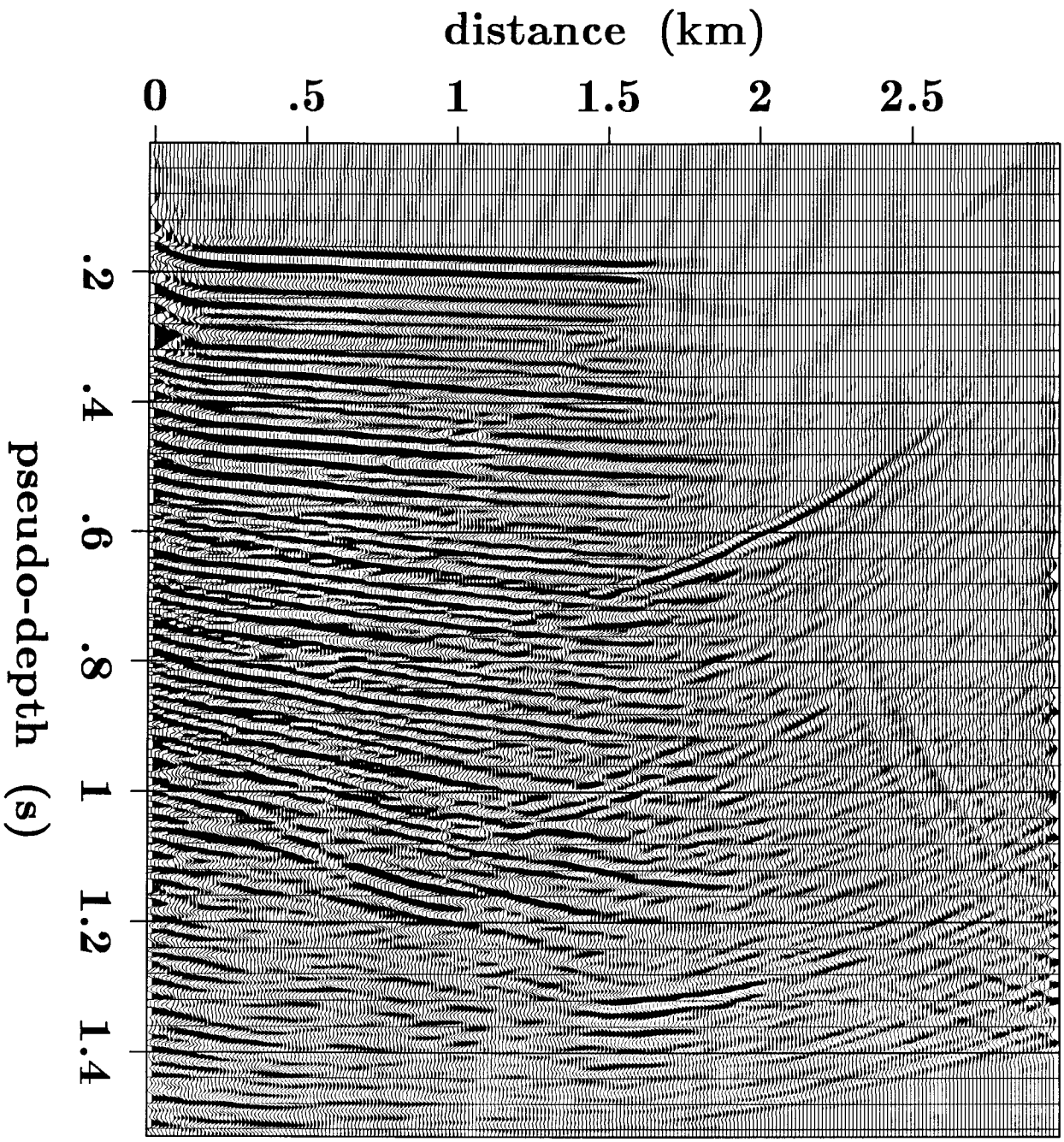

FIG. 5.8. Stacked section of migrated profiles. Boundary reflections and some incoherent noise are suppressed, while reflector images are enhanced. The fault plane is imaged with high resolution.

§ 5.3 VELOCITY INVERSION AND EXTRAPOLATION OF MULTIPLE REFLECTIONS

Velocity analysis by maximizing stacking power

Stacking migrated profiles over shot axis s using equation (5.6) yields the maximum power when the velocities used in the migrations are correct. Therefore, scanning through a range of velocities and maximizing the stacked power at a certain depth provides a method for picking the correct velocity at that depth. The same procedure can then be carried out to estimate velocities for the next depth of interest by downward extrapolating later arrivals through shallower depths using the known velocities estimated earlier and scanning through certain ranges of velocities for the deeper part of the section, until all velocities from the surface to the maximum depth of interest are obtained.

Under the assumption of local lateral homogeneity and a flat-layered medium (as in conventional velocity analysis from CMP gathers), velocity analysis of common-shot gathers is as simple as conventional velocity analysis of CMP gathers, since similar normal-moveout-correction formulas can be used, and we do not need to migrate and then stack to estimate velocity. However, this approach will produce RMS velocities of the earth instead of the interval velocities that can be obtained by the method of migration and stacking.

When velocity varies laterally, the method of migration and stacking should be used, though it is possible to apply moveout correction by ray tracing. Two approaches to velocity inversion can be taken in the method of migration and stacking. The first approach is to do constant-velocity migrations of all profiles and stacking, in a way similar to Toldi's scheme (Toldi, 1985) or Fowler's scheme (Fowler, 1984). The second approach is to invert velocity by perturbing the velocity model and iterating profile migrations.

Imaging multiple reflections and other types of waves

As discussed in section 5.1, LITWEQ profile migration images underground structures by cross-correlating downward continued primaries and downgoing incident waves, while suppressing incoherent noise, such as multiple reflections. If computations of both the forward modeling and the backward extrapolation are done over the whole rectangular region $0 \leq t \leq t_{\max}$ and $0 \leq \tau \leq \tau_{\max}$, as is the case in two-way LITWEQ modeling, then not only primary reflections but also multiple reflections may be

migrated to the proper reflector positions and become coherent.

§ 5.4 3-D POSTSTACK MIGRATION

Three-dimensional migration has been used in the processing of seismic data, especially land data, for many years. With the development of supercomputers, such as the Cray and the Convex, both the speed and the memory problems associated with 3-D migration have become less severe than they were before.

We have seen how the LITWEQ method can be applied to 2-D wavefield extrapolation. The same transformation as used in the 2-D LITWEQ method can be applied to the 3-D acoustic wave equation, giving a 3-D LITWEQ method.

The 3-D acoustic wave equation is

$$\frac{\partial^2 P}{\partial x^2} + \frac{\partial^2 P}{\partial y^2} + \frac{\partial^2 P}{\partial z^2} - \frac{1}{v^2}\frac{\partial^2 P}{\partial t^2} = 0 . \tag{5.7}$$

Transforming equation (5.7) with

$$\begin{cases} x' = x , \\ y' = y , \\ z' = \dfrac{1}{\sqrt{2}}(z - vt) , \text{ and} \\ t' = \dfrac{1}{\sqrt{2}}(z/v + t) \end{cases} \tag{5.8}$$

gives the resulting 3-D LITWEQ equation

$$\frac{\partial^2 P}{\partial x'^2} + \frac{\partial^2 P}{\partial y'^2} + \frac{2}{v}\frac{\partial^2 P}{\partial z' \partial t'} = 0 . \tag{5.9}$$

Equation (5.9) is exact when the velocity is constant. A 3-D LITWEQ method for a variable velocity medium can be derived similarly as the 2-D LITWEQ method for that medium was derived in section 3.4. There will be some more terms (reverberation and time-shifting terms) on the right-hand side of equation (5.9). To avoid redundancy and to simplify the following discussion, we will assume that these terms are negligible (the velocity gradient is small enough), so that equation (5.9) will also be valid for a variable velocity medium. Incorporating these terms into the discussion is not difficult, however (we did so in section 3.5).

There are several ways to implement the 3-D LITWEQ. The fastest and simplest implementation on a vector machine is to migrate data in the (k_x , k_y , z', t') domain when velocity changes only with depth, where k_x and k_y are Fourier duals of the

horizontal coordinates x and y, respectively. However, in laterally inhomogeneous media, the 3-D LITWEQ extrapolation has to be implemented in the (x, y, z', t') domain.

In laterally homogeneous media

When the velocity of medium can be regarded as a function of depth only, equation (5.9) can be transformed into the Fourier domain as

$$(k_x^2 + k_y^2)\, P - \frac{2}{v}\, \frac{\partial^2 P}{\partial z' \partial t'} = 0 . \tag{5.10}$$

Equation (5.10) can be solved by the explicit finite-difference scheme used in the 2-D (k_x, z', t') LITWEQ migration, treating the term $(k_x^2 + k_y^2)$ in the 3-D migration like k_x^2 in the 2-D migration.

Vectorization of scalar computation in a vector machine is difficult and relatively inefficient when there is recursive computation inside computation loops. Therefore, an implementation of equation (5.10) can take better advantage of a vector machine than an implementation of equation (5.9), since no recursive computation is involved in using equation (5.10).

Figure 5.9 shows an impulse response of a 3-D LITWEQ migration operator. The input is a spike at (x =32, y =32, z =25). The impulse response is a hemisphere.

In laterally inhomogeneous media

When velocity is varying laterally, implementation of the 3-D LITWEQ in (x', y', z', t') is needed. Both implicit and explicit finite-difference methods can be used to implement equation (5.9).

For the implicit method, unknowns that are solved simultaneously in the 3-D case lie on a plane, while unknowns in the 2-D case lie along a line. A matrix with a bandwidth of $(2n+1)$ needs to be solved at each step of 3-D extrapolation, where $n = \min(nx, ny)$ (nx and ny are the numbers of computational points in the x direction and the y direction, respectively). The huge memory required and the high cost of solving this large matrix equation make the algorithm practically infeasible, unless some splitting method is used. Other methods, such as the conjugate-gradient method or the steepest-descent method, can also be used.

The splitting and the full-separation methods use split equations of wave equation (5.9) to complete computation, even though their solutions are approximate when the velocity is not constant. Equation (5.9) can be split into two equations:

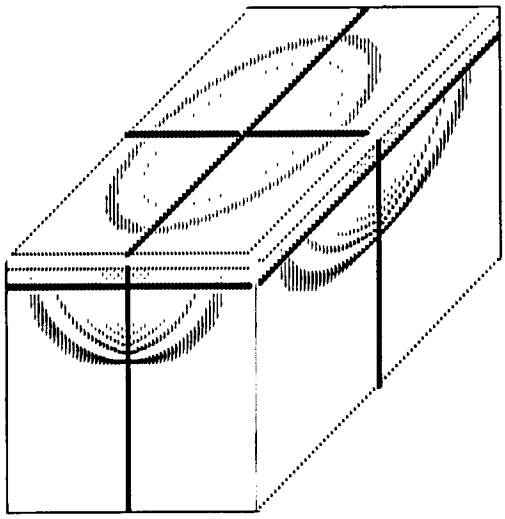

FIG. 5.9. Impulse response of 3-D LITWEQ migration. The input is a single spike at position (x =32, y =32, z =25).

$$\frac{\partial^2 P}{\partial x'^2} + \frac{1}{v}\,\frac{\partial^2 P}{\partial z' \partial t'} = 0\,, \tag{5.11}$$

and

$$\frac{\partial^2 P}{\partial y'^2} + \frac{1}{v}\,\frac{\partial^2 P}{\partial z' \partial t'} = 0\,. \tag{5.12}$$

The splitting methods (Claerbout, 1976; Botha and Pinder, 1983) solve equation (5.9) by alternatively solving equation (5.11) and equation (5.12) at each step of extrapolation in (z', t'). Hence, the well-known implicit scheme for 2-D migration can be used in this approach. Splitting equations more accurate than equations (5.11) and (5.12) can be used to obtain higher accuracy at higher computational cost (Mitchell and Griffiths, 1980).

By using the full-separation method (Mitchell and Griffiths, 1980; Claerbout ,1985), we can solve equation (5.9) by solving equation (5.11) for all steps in (z', t') first, and then solving equation (5.12) again in (z', t'). This method requires the velocity of medium to be constant. Errors will occur in this method when the velocity varies spatially.

Both the splitting and the full-separation methods use recursive computation when the implicit scheme is used. Recursive computation greatly reduces the efficiency of optimization and vectorization of scalar computation by vector computers.

More about the 2-D LITWEQ transformation

We can also transform the 2-D acoustic wave equation with

$$\begin{cases} x' = x + z + \sqrt{2}vt \ , \\ z' = x + z - \sqrt{2}vt \ , \text{ and} \\ t' = \dfrac{-1}{v}(-x + z) + \sqrt{2}t \ , \end{cases} \tag{5.12}$$

resulting in the equation

$$2\frac{\partial^2 P}{\partial x' \partial z'} - \frac{1}{v}\frac{\partial^2 P}{\partial x' \partial t'} + \frac{1}{v}\frac{\partial^2 P}{\partial z' \partial t'} = 0 \ , \tag{5.13}$$

which can use a compact, eight-point, finite-differencing star pattern to solve the equation.

§ 5.4 SUMMARY

The LITWEQ wavefield extrapolation method can be applied to prestack migration of seismic data. Both the problem of extrapolating steeply dipping reflections and that of handling lateral inhomogeneity can be solved by the LITWEQ method. Further applications of the LITWEQ method can be expected in seismic inversion, multiple-reflection extrapolation, 3-D wavefield extrapolation and tomography.